

Pressure dependence of interfacial resistance in pellets made from GeS 2 -Ga 2 S 3 -Li 2 S-LiI glass powder

Bo Fan, Bai Xue, Zhongkuan Luo, Xianghua Zhang, Hongli Ma, Laurent Calvez

▶ To cite this version:

Bo Fan, Bai Xue, Zhongkuan Luo, Xianghua Zhang, Hongli Ma, et al.. Pressure dependence of interfacial resistance in pellets made from GeS 2 -Ga 2 S 3 -Li 2 S-LiI glass powder. Journal of the American Ceramic Society, 2019, 102 (3), pp.1122-1127. 10.1111/jace.15954. hal-01952837

HAL Id: hal-01952837 https://univ-rennes.hal.science/hal-01952837

Submitted on 12 Dec 2018

HAL is a multi-disciplinary open access archive for the deposit and dissemination of scientific research documents, whether they are published or not. The documents may come from teaching and research institutions in France or abroad, or from public or private research centers. L'archive ouverte pluridisciplinaire **HAL**, est destinée au dépôt et à la diffusion de documents scientifiques de niveau recherche, publiés ou non, émanant des établissements d'enseignement et de recherche français ou étrangers, des laboratoires publics ou privés.

DR BAI XUE (Orcid ID: 0000-0001-8246-6717)

Article type : Article

Editor : Professor Pierre Lucas

Pressure dependence of interfacial resistance in pellets made from $GeS_2\text{-}Ga_2S_3\text{-}Li_2S\text{-}LiI \ glass \ powder$

Bo Fan^a, Bai Xue^{a*}, ZhongkuanLuo^b, XianghuaZhang^{c*}, Hongli Ma^c, Laurent Calvez^c

^a Shenzhen Key Laboratory of Advanced Thin Films and Applications, College of Physics & Energy, Shenzhen University, Shenzhen, 518060, China

^b Shenzhen Key Laboratory of New Lithium-ion Battery and Mesoporous Materials, College of Chemistry and EnvironmentalEngineering, Shenzhen University, Shenzhen, 518060, China

^cLaboratory of Glasses and Ceramics, Institute of Chemical Science, University of Rennes 1, Rennes 35042, France

Abstract

The interfacial resistance and capacitance in pellets made from GeS₂-Ga₂S₃-Li₂S-LiI glass powder are studied under uniaxial compression. By varying the pressure, remarkable change of the geometric dimension of the interfacial resistance and capacitance is observed. Assuming that the interfacial resistance and capacitance arise from the contact region between the powder particles, a quantitative model is established that well describes the

geometric dimension change of the interfacial resistance and capacitance. This work emphasizes that ameliorating the contact between the particles is one of the most important methods to reduce the interfacial resistance in the powder-type ionic-conduction devices made from highly-conductive sulfide solid electrolyte powders.

Keywords: chalcogenide glass, lithium ionic conductivity; solid electrolyte; interfacial resistance;

* Corresponding author.Tel: +86 (0)755 26534995

E-mail address:baixue@szu.edu.cn, xiang-hua.zhang@univ-rennes1.fr

1.Introduction

Sulfide solid electrolytesshow excellent ionic conductivity ^{1, 2} and are of great potential for applying in solid-state batteries ^{3, 4, 5}. Different from its oxide counterpart, the influence interfacial/grain boundary resistance on the total conductivity in sulfide solid electrolytes is normally considered to be negligible ⁶. However, recent researches confirm that once the conductivity of the sulfide electrolyte reaches 10⁻³ S/cm or more, the interfacial/grain boundary resistance turns out to be a crucial factor for the ionic conductivity ^{7, 8}.

To be applied in solid-state batteries, sulfide solid electrolytes are typically used in the form of powder. For example, mixtures of active material powders, solid electrolyte powders and carbon are widely used as composite cathodes ^{9, 10, 11}. Additionally, pellets cold-pressed

from the solid electrolyte powders are used as the ion-transport layers which separate the anode and the cathode ¹². In such powder-type solid-state batteries, there exists a large amount of interface. Despite the importance of interfacial resistance to the application, deep discussions about the origin of interfacial resistance in sulfide solid electrolyte are rarely reported in the literatures. GeS₂-based glasses are of good chemical and thermal stability ¹³, ¹⁴. By the addition of lithium, the ionic conductivity of this glass system can reach 10⁻⁴ S/cm, and can be further improved to 10⁻³ S/cm by the addition of LiI ^{15, 16}. In this paper, the interfacial resistance in the pellets made from ionic-conductive GeS₂-Ga₂S₃-Li₂S- LiI glass powder is studied under varying uniaxial compression. This study helps us to understand the origin of the interfacial resistance in this sulfide solid electrolyte. A simple model is proposed to describe the observed pressure dependence of the interfacial resistance.

2. Experimental procedures

32GeS₂-8Ga₂S₃-40Li₂S-20LiI (in mol%) glass powders were prepared by ball milling. Starting materials, Ge (99,99%, Alfa Aesar), Ga (99.99%, Alfa Aesar), S (99%, Alfa Aesar) and Li₂S (99.9%, Alfa Aesar) were weighed according to the glass composition. Then 8 g starting materials were put into a tungsten carbonide jar with ten tungsten carbonide grinding balls (φ=10mm). The filling rate is about 1/3. The ball milling was conducted at 600 rpm using a planetary ball mill apparatus (Pulverisette 7, Fritsch GmbH, Germany). The duration of ball milling was 62 h. All the operations were conducted in an Ar-filled glove box.

X-ray diffraction (D8 Advance, Bruker AXS GmbH, Germany) were used to monitor the amorphization degree of the ball-milling product. Raman spectra were recorded by a Raman spectrometer (inVia, Renishaw Inc., UK) with a 532 nm DPSS laser as the source. The as-prepared glass powders were cold-pressed into pellets under 330 MPa (~15 mm diameter and ~1.4 mm thickness) in anAr-filled glove box. The pellets were then sealed in silica tubes which were pumped to high vacuum (8×10⁻⁴ Pa). The pellets were sintered under vacuum at 240 °C for 10 h to improve the density. Finally, the pellets were coated by Au films on top and bottom surfaces for conductivity measurement. The coating was carried out with a low vacuum coater (EM ACE200, Leica Microsystems, Germany) which was installed inside an Ar-filled grove box. The morphology of the sintered pellets was recorded by a scanning electron microscope (Zeiss supra 55, Carl Zeiss GmbH, Germany). The sample preparation was carefully conducted to avoid direct air exposure. Only a transient air contactoccurredduring the sample installation of SEM characterization, which might have slight influence on the recorded sample morphology images.

The ionic conductivity was measured using an AC impedance method in an argon filled glove box, using a frequency response analyzer (Solartron 1260A, SolartronAnalytical Inc., UK). A tablet press machine is modified to be used as the sample holder so that varying uniaxial compression can be applied onto the samples during the conductivity measurement.

3. Results and discussions

The XRD pattern of the 62 h ball-milling product is shown in Figure 1(a). No diffraction peaks are detected in the sample, indicating that the sample is thoroughly amorphized. Figure 1(a) also shows the XRD pattern of the pellet sintered at 240°C for 10 h. The absence of diffraction peaks of this sintered pellet confirms that the crystallization is negligible during the sintering process.

Figure 1(b) shows the Raman spectra of the as-milled 32GeS₂-8Ga₂S₃-40Li₂S-20LiI glassy powder and the pellet sintered at 240 °C for 10 h. Two spectra have similar features. The broad Raman signal is principally composed of two peaks: the peak around 350 cm⁻¹, which is attributed to the vibration of [GeS_{4/2}] tetrahedrons, and the peak around 407 cm⁻¹, which is attributed to the vibration of [GeS_{2/2}S₂²⁻] tetrahedrons ¹. This is a typical Raman signal for GeS₂-based glasses.Raman spectra indicate that no significant structural evolution takes place during the sintering, that is accordant with the XRD results.

By applying different uniaxial compression, the impedance spectra of one sample pellet were measured and are presented in Figure 2. All the spectra consist of a high-frequency arc and a low-frequency tail, manifesting ionic conductive behaviour. The arc is attributed to the parallel of the interfacial capacitance C_{if} and the interfacial resistance R_{if} , while the tail, a typical signal of a Warburg element W_{el} , is attributed to the diffusion of ions near the electrolyte/electrode interface ¹⁷. The intragrain resistance R_{ig} can be obtained at the high frequency end of the arc, and the sum of R_{ig} and R_{if} can be obtained at the low frequency end of the arc. Evidently Figure 2 shows that the dimension of the arc decreases with the increasing applied pressure, which indicates a remarkable decrease of R_{if} under compression.

To precisely characterize the parameters R_{ig} , R_{if} and C_{if} , the impedance spectra are fitted with a typical equivalent circuit for solid electrolytes, as shown in the insert of Figure 2. The fitting results are listed in Table 1. When the applied pressure increases from 0 to 330 MPa, the intragrain resistance R_{ig} decreases slightly. Quite differently, the pressure dependence of the interfacial resistance R_{if} and the interfacial capacitance C_{if} is evident.

The pressure dependence of the ionic conduction was also reported in other ionic conductors, as summarized in Table 2. It was observed that in high purity Y₂O₃-stabilized tetragonal zirconia ceramics (YTZ), by applying a 270 MPa pressure, both intragrain and interfacial resistances changed about 8% ¹⁸. In this case, the interfacial resistance is principally ascribed to the space-charge layers at the grain boundary, according to the Frenkel's model ¹⁷. It is proposed that under pressure the deformation of YTZ reduces the interionic space, limits the ion mobility and consequently changes the resistance ¹⁹. Since the mechanical deformation is small, the pressure dependence of the ionic conduction is not evident. Additionally, based on the space-charge layer postulation, bulk and grain boundary form a unique mechanical entity, so that intragrain and interfacial resistances show identical behavior under pressure.

It is worth noting that in our case, the interfacial ionic conduction change is as high as 1666%, far more pronounced than the intragrain. Therefore, the interfacial resistance of the glass powder in this study cannot be simply ascribed to the space-charge layers or a secondary interfacial phase. Actually, the space-charge layers are typically built with charged lattice defects, whichare usually absent in glass materials. A similar phenomenon was observed in Li₂S-P₂S₅ glass, where the ionic conductance increased more than 420% after

applying 360 MPa pressure ²⁰. Such an evident increment can be attributed to the densification of the sample pellets by cold-pressing. Therefore, we propose that the highly pressure-dependent interfacial resistance of our sulfide glass pellets is intimately associated with a geometrical factor, the pore distribution in the pellets.

As well known, the resistance and the capacitance are determined by both the material parameters such as resistivity ρ and permittivity ε_r , and the geometric parameters such as area and thickness. Since the maximal applied pressure is 330 MPa that is too low to evidently change ρ or ε_r (as demonstrated in Ref. 18), the significant decrease of R_{if} and the increase of C_{if} indicate that the pressure evidently changes the geometric dimension of the two elements.

Viewing the significant geometric dimension change of the interfacial resistance and capacitance under compression and considering the influence of pore distribution on the interfacial resistance, a model is proposed for the interfacial resistance in pellets made from GeS_2 - Ga_2S_3 -Li₂S-LiI glass powder, which is schemed in Figure 3. For simplification of the modeling, it is assumed that the powder particles are spheres with identical size, and are close-packed so that they are in a hexagonal arrangement (Figure 3(b)). Due to the presence of compression or sintering, the contact region between the powder particles deforms.

Geometrically, such deformation is described by the overlap of the powder spheres.

Consequently, a porous morphology appears (Figure 3(b)). The porous morphology as described by the model is coincident well with the real morphology of the sample pellets, which is illustrated by the SEM image in Figure 3(a).

Here we focus on the contact region between two particles (Figure3(c)). Because of the imperfect contact between the particles, the ion transport path shrinks in the contact region. We propose such a shrinkage is the major origin of the interfacial resistance. Therefore, the interfacial resistance has the same resistivity ρ_i as the intragrain resistance. As for the geometric dimension, the area A of the interfacial resistance is roughly the area enveloped by the intersection of the two powder spheres, and its thickness is the thickness of the contact region 2w. The geometric dimension of the interfacial resistance is colored by red in Figure3(c). Thus, the resistance of a single interfacial can be expressed as follow:

$$R_{\rm if}^{\rm s} \approx \frac{\rho_i \times 2w}{A}$$
 (1)]

A and wis geometrically related by the following equation:

$$A = \pi \left[r^2 - (\frac{\sqrt{3}}{2} r + w)^2 \right]$$
 (2)

where r is the radius of the powder sphere.

The interfacial capacitance is proposed to be contributed from both the intergranular contact region (red in Figure3(c)) and the air in the voids (bluein Figure3(c)). The area of interfacial capacitance is fixed as A', while the thickness 2w varies with different applied pressure. The ratio between w and r, defined as the reduced interfacial width w^* , can be calculated from the intragrain capacitance C_{ig} and the interfacial capacitance C_{if} , by the following equation:

$$w^* \equiv \frac{w}{r} = \frac{C_{ig}}{C_{if}} \cdot \frac{\varepsilon_{if}}{\varepsilon_{ig}} = \frac{\varepsilon_{if}\varepsilon_0 S}{C_{if}t}$$
(3)

where ε_0 is the vacuum dielectric constant, ε_{if} is the average permittivity of interface, ε_{ig} is the permittivity of particle, S and t are respectively the area and thickness of the sample pellet. The reduced interfacial width under different pressure is calculated and listed in Table 1. It decreases with the applied pressure (the overlap between the powder spheres becomes more evident), reflecting the densification of the pellet under uniaxial compression.

According to the SEM image in Figure3(a), the interfacial width 2w, which is associated with the pore size, is about 40 nm, and the average powder (cluster) size 2r is about 500 nm. The reduced interfacial width w^* in the pressure-free sample could be estimated to be 0.08, and results in an interfacial capacitance of about 10^{-10} F. The value coincides well with the experimental data listed in Table 1. A typical interfacial capacitance in polycrystalline solid electrolytes with similar sample size is about 10^{-9} F, higher than the one observed in our samples. It is because that the interfacial layers caused by space-charge layer or secondary phase is typically thinner than the ones caused by poor particle-contact as discussed above.

Since the geometric parameters A and w of the interfacial resistance are all associated with the reduced interfacial width w^* , rearranging Equation (1) - (2) gives the relationship between the interfacial conductance G_{if} and the reduced interfacial width w^* :

$$G_{\rm if} = \frac{1}{R_{\rm if}} \propto \frac{1 - (\sqrt{3}/2 + w^*)^2}{w^*}$$
 (4)

Figure 4 shows the normalized interfacial conductance G_{if} versus reduced interface width w^* in two pellet samples. The relationship described by Expression (4) is also plotted in Figure 4. It can be seen that the modeling curve well predicts the trend of the experimental data. Thus, the model proposed above can well explain the pressure dependence of the

interfacial resistance and capacitance: On one hand, under high pressure, the width of the contact region between the particles decreases evidently. As a result, the thickness of the interfacial capacitance decreases so that the capacitance increases; On the other hand, high pressure improves the contact area between the particles, so that the ion transport path across the interface is enlarged. Consequently, the area of the interfacial resistance increases and lower resistance can be observed. The predicted curve somehow deviates from the experimental data under high pressure with low w^* . It might be caused by the simplicity of our geometric assumption that is inaccurate when large deformation of the particles occurs under high pressure.

The modeling curve in Figure 4 also predicts that by further reducing the interfacial width, the interfacial conductance can be rapidly improved. However, further reduction of w^* by the increase of applied pressure seems to be difficult and ineffective. Sintering techniques such as hot-pressing or SPS are expected to be a more effective way to improve the interfacial conductance. This conclusion is coincident with the experimental study on $\text{Li}_7\text{P}_3\text{S}_{11}$, whose ionic conductivity can be raised one order of magnitude by an optimized heat treatment in comparison with the cold-pressed samples 21 .

4. Conclusions

In summary, this work demonstrates that in the pellets made from GeS_2 - Ga_2S_3 - Li_2S -LiI glass powder , the geometric dimension of the interfacial resistance and capacitance can change remarkably under compression. To explain such a phenomenon, it is proposed that the interfacial resistance arises from the boundary region where good intergranular contact is

established, and the interfacial capacitance is contributed from both the intergranular contact region and the air in the voids. Since the contact region deforms under compression, its thickness is reduced and the contact area is enlarged. That's the reason for the geometric dimension change of the interfacial resistance and capacitance. Moreover, a quantitative model is successfully established to describe this geometric dimension change. This work indicates that ameliorating the contact between the particles is essential to reduce the interfacial resistance in the powder-type ionic-conduction devices made from highly-conductive sulfide solid electrolytes. Sintering techniques such as hot-pressing or SPS may be necessary to achieve this goal.

Acknowledgement

This work is the financially supported by the National Natural Science Foundation of China (No. 61504085/51702216), the Natural Science Foundation of Guangdong Province (No. 2017A030313325), and the Natural Science Foundation of Shenzhen University (No. 827-000037/201520).

References

- 1. Liu D, Zhu W, Feng Z, Guerfi A, Vijh A, and Zaghib K. Recent progress in sulfide-based solid electrolytes for Li-ion batteries. Materials Science and Engineering: B. 2016; 213: 169-76.
- Bachman J, Muy S, Grimaud A, Chang H-H, Pour N, Lux SF, et al. Inorganic solid-state electrolytes for lithium batteries: mechanisms and properties governing ion conduction. Chem Rev. 2016; 116: 140–162.
- 3. Han F, Yue J, Fan X, Gao T, Luo C, Ma Z, et al. High-performance all-solid-state lithium–sulfur battery enabled by a mixed-conductive Li₂S nanocomposite. Nano Lett. 2016; 16: 4521-27.
- Yamada T, Ito S, Omoda R, Watanabe T, Aihara Y, Agostini M, et al. All solid-state lithium–sulfur battery using a glass-type P₂S₅–Li₂S electrolyte: benefits on anode kinetics. J Electrochem Soc. 2015; 162: A646-A51.
- Lin Z, Liu Z, Fu W, Dudney NJ, Liang C, Lithium polysulfidophosphates: a family of lithium-conducting sulfur-rich compounds for lithium-sulfur batteries. Angew Chem Int Ed. 2013; 52: 7460-63.
- 5. Tatsumisago M, Nagao M, Hayashi A, Recent development of sulfide solid electrolytes and interfacial modification for all-solid-state rechargeable lithium batteries. Journal of Asian Ceramic Societies. 2013; 1: 17-25.
- 7. Xu RC, Xia XH, Yao ZJ, Wang XL, Gu CD, Tu JP, Preparation of Li₇P₃S₁₁ glass-ceramic electrolyte by dissolution-evaporation method for all-solid-state lithium ion batteries. Electrochim Acta. 2016; 219: 235-40.
- 8. Wei J, Kim H, Lee DC, Hu R, Wu F, Zhao H, et al. Influence of annealing on ionic transfer and storage stability of Li₂S–P₂S₅ solid electrolyte. J Power Sources. 2015; 294: 494-500.

- 9. Ohtomo T, Hayashi A, Tatsumisago M, Tsuchida Y, Hama S, Kawamoto K. All-solid-state lithium secondary batteries using the 75Li₂S·25P₂S₅ glass and the 70Li₂S·30P₂S₅ glass–ceramic as solid electrolytes. J Power Sources. 2013; 233: 231-35.
- Nagata H, Chikusa y. All-solid-state lithium—sulfur battery with high energy and power densities at the cell level. Energy Technology. 2016; 4: 484-89.
- 11. Xu R, Wu Z, Zhang S, Wang X, Xia Y, Xia X, et al. Construction of all-solid-state batteries based on a sulfur-graphene composite and Li_{9.54}Si_{1.74}P_{1.44}S_{11.7}Cl_{0.3} solid electrolyte. Chemistry A European Journal. 2017; 23: 13950-56.
- 12. Nagao M, Hayashi A, Tatsumisago M. Sulfur–carbon composite electrode for all-solid-state Li/S battery with Li₂S–P₂S₅ solid electrolyte. Electrochim Acta. 2011; 56: 6055-59.
- Cozic D, Bréhault A, Coq DL, Usuki T. GeS₂–Ga₂S₃–LiCl glass system: electrical conductivity and structural considerations. Int J Appl Glass Sci. 2016; 7: 513-23.
- 14. Xu Y, Zhang Q, Shen C, Chen D, Zeng H, Chen G. Broadband near- IR emission in $Tm/Er-\ codoped\ GeS_2-In_2S_3-\ based\ chalcohalide\ glasses.\ J\ Am\ Ceram\ Soc.\ 2009;\ 92(12):$ 3088-91.
- 15. Saienga J, Kim Y, Campbell B, Martin SW. Preparation and characterization of glasses in the LiI+Li₂S+GeS₂+Ga₂S₃ system. Solid State Ionics. 2005; 176: 1229-36.
- Saienga J, Martin SW. The comparative structure, properties, and ionic conductivity of LiI + Li₂S
 + GeS₂ glasses doped with Ga₂S₃ and La₂S₃. J Non-Cryst Solids. 2008; 354: 1475-86.
- Barsoukov E, Macdonald JR. Impedance Spectroscopy: Theory, experiment, and applications.
 Second Edition . John Wiley & Sons, Inc.: Hoboken, NJ, USA; 2005.

- 18. M'Peko JC, Souza MF. Ionic transport in polycrystalline zirconia and Frenkel's space-charge layer postulation. Appl Phys Lett. 2003; 83: 737-39.
- 19. M'Peko JC, Spavieri Jr. DL, Souza MF. In situ characterization of the grain and grain-boundary electrical responses of zirconia ceramics under uniaxial compressive stresses. Appl Phys Lett. 2002; 81: 2827-29.
- 20. Sakuda A, Hayashi A, Tatsumisago M. Sulfide solid electrolyte with favorable mechanical property for all-solid-statelithium battery. Sci Reports. 2013; 3: 2261.
- 21. Seino Y, Ota T, Takada K, Hayashi A, Tatsumisago M. A sulphide lithium super ion conductor is superior to liquid ion conductors for use in rechargeable batteries. Energy Environ Sci. 2014; 7: 627-31.

Table and Figure Captions

Table 1.Intragrain resistance R_{ig} , interfacial resistance R_{if} , interfacial capacitance C_{if} , and reduced interface width w^* of one pellet under different pressure. All the parameters are deduced from the impedance spectra in Figure 2.

Table 2. Pressure dependence of ionic conductivity in the studied pellet sample and in other ionic conductive glasses and ceramics.

Figure1.(a) XRD patterns and (b) Raman spectra of the as-milled glass powder and the pellet sintered at 240°C for 10 h.

Figure2. Impedance spectra of one sample pellet measured under varying uniaxial compression. The curves from right to left are recorded under the pressure of 0 MPa, 55 MPa, 110 MPa, 165 MPa, 220 MPa, 275 MPa and 330 MPa, respectively. The equivalent circuit is inserted.

Figure3. Morphology of the pellets made from GeS₂-Ga₂S₃-Li₂S-LiI glass powder and schematic diagrams of the model for the interfacial resistance. (a) SEM image of the pellets showing the porous morphology. (b) The powders are assumed to be close-packed so that they are in a hexagonal arrangement. (c) The interfacial resistance arises from the boundary region where good intergranular contact is established (red region), and the interfacial capacitance is contributed from both the intergranular contact region (red region) and the air in the voids (blue region).

Figure4. Normalized interfacial conductance G_{if} versus reduced interface width w^* . The solid line is calculated by the proposed model for the interfacial resistance.

•

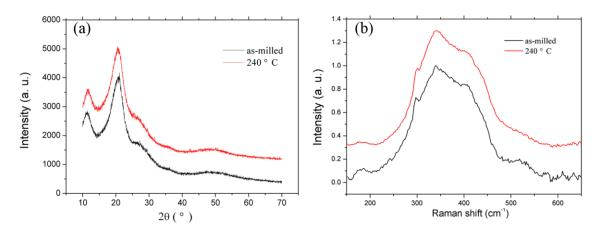
Table 1. Intragrain resistance R_{ig} , interfacial resistance R_{if} , interfacial capacitance C_{if} , and reduced interface width w^* of one pellet under different pressure. All the parameters are deduced from the impedance spectra in Figure 2.

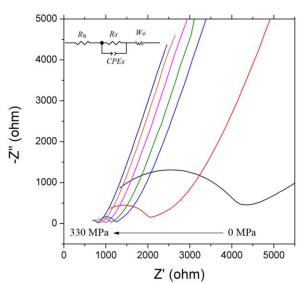
Pressure	$R_{ m ig}$	$R_{ m if}$	$C_{ m if}$	w*
(MPa)	(ohm)	(ohm)	(pF)	
0	866	3072	164	0.0679
55	848	1105	329	0.0340
110	871	313	655	0.0171
165	805	276	672	0.0166
220	738	214	874	0.0128
275	671	174	1060	0.0105
330	624	152	1215	0.0092

Table 2. Pressure dependence of ionic conductivity in the studied pellet sample and in other ionic conductive glasses and ceramics.

Material	Applied Pressure (MPa)	$ (\sigma - \sigma_0)/\sigma_0 $		Reference
		intragrain	interface	
GeS ₂ -Ga ₂ S ₃ -Li ₂ S-LiI glass	275	29%	1666%	This work
YTZ	270	8%	8%	[18]
Li ₂ S-P ₂ S ₅ glass	360		>420% *	[20]

^{*} The relative conductivity change induced by pressure in $\text{Li}_2\text{S}-\text{P}_2\text{S}_5$ glass is calculated with the total conductivity measured under 40 MPa and 360 MPa. The total conductivity is mainly determined by interfacial conductivity in this material 20 .





(b)

